

Seismic Catastrophe in Japan on March 11, 2011: Long-Term Prediction on the Basis of Low-Frequency Microseisms

A. A. Lyubushin

Schmidt Institute of Physics of the Earth, Russian Academy of Sciences, ul. Bol'shaya Gruzinskaya 10, Moscow, 123995 Russia
e-mail: lyubushin@yandex.ru

Abstract—This paper presents a software technique for analyzing the multidimensional time series of microseismic oscillations on the basis of over 14 years of continuous observations, from early 1997 to February 2011, at F-net (Japan) broadband seismic stations. An analysis of the multifractal parameters of low-frequency microseismic noise allowed us to hypothesize, in as early as 2008, that Japanese Islands were approaching a large seismic catastrophe, the signature of which was a statistically significant decrease in the support width of the multifractal singularity spectrum. Subsequently, as new data became available and after some new statistics of microseismic noise (such as a logarithm of noise variance and an index of linear predictability) were included in joint analysis, we obtained some new results, indicating the facts that the parameters of the microseismic background had been increasingly synchronized (the synchronization process was estimated to start in mid-2002) and that the seismic danger had permanently grown. A cluster analysis of background parameters led us to conclude that in mid-2010 the islands of Japan entered a critically dangerous developmental phase of seismic process. The prediction of the catastrophe, first in terms of approximate magnitude (mid-2008) and then in terms of approximate time (mid-2010), was documented in advance in a series of papers and in proceedings at international conferences.

Keywords: synchronization, microseismic background, multifractals, earthquake precursors.

DOI: 10.1134/S0001433811080056

INTRODUCTION

Low-frequency microseismic oscillations are an important source of information on the processes in the earth's crust, despite the fact that the main energy of these oscillations is generated by processes in the atmosphere and ocean such as variations in the atmospheric pressure and the effect of oceanic waves on the coast and shelf. The interrelation between low-frequency microseisms with periods of 5–500 s and the intensity of oceanic waves has been studied extensively in works [Friedrich et al., 1998; Kobayashi and Nishida, 1998; Tanimoto et al., 1998; Tanimoto and Urn, 1999; Ekstrom, 2001; Tanimoto, 2001, 2005; Berger et al., 2004; Rhie and Romanowicz, 2004, 2006; Kurrle and Widmer-Schmidrig, 2006; Stehly et al., 2006]. In effect, the earth's crust is a medium where the energy of atmospheric and oceanic processes propagates and, because the transfer properties of the crust depend on the crustal state, the statistical properties of microseisms reflect changes in the properties of the lithosphere.

This intrinsically simple idea behind the use of low-frequency microseismic oscillations for lithospheric monitoring is, nonetheless, not as straightforward to implement. The main difficulty stems from the fact that data are subject to strong effects from a large number of uncorrelated sources which are often distributed diffusely over the earth's surface. Therefore, while

studying the transfer properties of the lithosphere, the input effect and response cannot be simultaneously controlled in this case. Moreover, separation into “signal” and “noise,” while standard for traditional methods of data analysis, makes no sense in processing microseismic oscillations. Only tidal variations in the microseism amplitude, as well as the onsets and codes of well-known strong earthquakes, can be referred to a priori as a “signal.” These signals have been used in geophysics applications for a long time. All the other variations in the microseisms “got lost in the noise.”

A spectral analysis, which is traditionally used in geophysical noise studies, is a bad choice because noise contains neither monochromatic components nor narrowband signals. Therefore, the approach suggested here uses the apparatus of multifractal singularity spectra for analysis [Mandelbrot, 1982; Feder, 1988], which makes it possible to describe the noise structure most adequately. The singularity spectra were estimated in works [Kantelhardt et al., 2002; Ramírez-Rojas et al., 2004; Currenti et al., 2005; Ida et al., 2005; Telesca et al., 2005; Lyubushin and Sobolev, 2006; Lyubushin, 2007, 2008c] to analyze the geophysical time series.

It should be stressed that the situation with this event was very specific in that it was predicted far in advance of the actual seismic catastrophe in a few publications [Lyubushin, 2009, 2010d, 2011] (the last

paper submitted in late April 2010) and in the proceedings of international conferences [Lyubushin, 2008a, b, 2010a, b, c]; it was also mentioned in application form submitted to the Russian Expert Society for the Prediction of Earthquakes and Seismic Hazards on April 26, 2010.

Below we successively describe the stages of data processing and processing results which allowed us to predict the impending catastrophe and estimate the time of the strongest earthquake.

INITIAL DATA: F-net NETWORK

Data from the broadband seismic F-net network are publicly available online (<http://www.hinet.bosai.go.jp/fnet>). The total number of stations is 83. The data analyzed are vertical components with a 1-s time step (LHZ records); they contain gap intervals as well as incorrect data (of the type of the constant zero values) due to failures of measuring and recording instrumentation. We considered only stations poleward of 30° N and, thereby excluding the data from six solitary stations located on remote small islands. The locations of the other 77 stations are indicated in Fig. 1 by numerals from 1 to 5, meaning that the stations belong to five spatial clusters; the numbers of the stations in each cluster is also given. The stations are spatially clustered in order to (1) facilitate the spatial averaging of parameters of microseisms (by determining a median value over the stations) and (2) to ensure the continuity of the cluster-average values (there were many stations and several per cluster were always operating).

THE PARAMETERS OF THE SINGULARITY SPECTRUM OF LOW-FREQUENCY MICROSEISMS

Below we outline the technical details of the used estimates of the singularity spectrum [Lyubushin and Sobolev, 2006; Lyubushin, 2007, 2008c]. One important element of this estimate is to use local polynomials to remove scale-dependent trends; this allows us to eliminate deterministic trends (tidal and temperature variations in our case) and analyze only high-frequency pulsations of the series, i.e., the noise component.

Let $X(t)$ be a random process. We define the sweep $\mu_X(t, \delta) = \max_{t \leq s \leq t+\delta} X(s) - \min_{t \leq s \leq t+\delta} X(s)$ as a measure of the behavior of the signal $X(t)$ on the interval $[t, t + \delta]$ and calculate the average modulus of these measures raised to power q :

$$M(\delta, q) = M\{(\mu_X(t, \delta))^q\}. \quad (1)$$

A random process is called scale-invariant if $M(\delta, q) \sim |\delta|^{\kappa(q)}$ as $\delta \rightarrow 0$; i.e., there is a limit

$$\kappa(q) = \lim_{\delta \rightarrow 0} \frac{\ln M(\delta, q)}{\ln |\delta|}. \quad (2)$$

If $\kappa(q)$ is a linear function, i.e., $\kappa(q) = Hq$, where $H = \text{const}$, $0 < H < 1$, then the process is called a monofractal process [Taqqu, 1988].

The DFA method [Kantelhardt et al., 2002] can be used to evaluate the function $\kappa(q)$ on a finite sample of the time series $X(t)$, $t = 1, \dots, N$. Let s be the number of readings, associated with the varied scale δ_s : $\delta_s = s \Delta t$. We divide the sample into nonoverlapping small intervals with the length of s readings

$$I_k^{(s)} = \{t : 1 + (k-1)s \leq t \leq ks, \quad k = 1, \dots, [N/s]\}, \quad (3)$$

$$y_k^{(s)}(t) = X((k-1)s + t), \quad t = 1, \dots, s \quad (4)$$

is a fragment of the time series $X(t)$ corresponding to the interval $I_k^{(s)}$. Let $p_k^{(s,m)}(t)$ be the m th order polynomial, fitted to the signal $y_k^{(s)}(t)$ by the least squares method. We now consider deviations from the local trend:

$$\Delta y_k^{(s,m)}(t) = y_k^{(s)}(t) - p_k^{(s,m)}(t), \quad t = 1, \dots, s, \quad (5)$$

and evaluate the quantity

$$Z^{(m)}(q, s) = \left(\sum_{k=1}^{[N/s]} (\max_{1 \leq t \leq s} \Delta y_k^{(s,m)}(t) - \min_{1 \leq t \leq s} \Delta y_k^{(s,m)}(t))^q / [N/s] \right)^{1/q}, \quad (6)$$

to be considered an estimate for $(M(\delta_s, q))^{1/q}$. We define the function $h(q)$ as a coefficient of the linear regression between $\ln(Z^{(m)}(q, s))$ and $\ln(s)$: $Z^{(m)}(q, s) \sim s^{h(q)}$. Obviously, $\kappa(q) = qh(q)$; $h(q) = H = \text{const}$ for a monofractal process.

After the function $\kappa(q)$ is determined, the next step in the multifractal analysis [Feder, 1988] is to calculate the singularity spectrum $F(\alpha)$, which can be defined as a fractal dimension of the time instants τ_α , having one and the same Gelder–Lipschitz parameter: $\lambda(t) =$

$\lim_{\delta \rightarrow 0} \frac{\ln(\mu(t, \delta))}{\ln(\delta)}$, i.e., $\lambda(\tau_\alpha) = \alpha$. A standard approach

is to calculate the statistical Gibbs sums

$$W(q, s) = \sum_{k=1}^{[N/s]} (\max_{1 \leq t \leq s} \Delta y_k^{(s,m)}(t) - \min_{1 \leq t \leq s} \Delta y_k^{(s,m)}(t))^q, \quad (7)$$

and to determine the mass index $\tau(q)$ from the condition $W(q, s) \sim s^{\tau(q)}$, whereupon the $F(\alpha)$ spectrum is calculated from the formula

$$F(\alpha) = \max_q \{\min(\alpha q - \tau(q)), 0\}. \quad (8)$$

From a comparison of Eqs. (6) and (7), it can be easily seen that $\tau(q) = \kappa(q) - 1 = gh(q) - 1$. Thus, $F(\alpha) = \max_q \{\min(q\alpha - h(q)) + 1, 0\}$.

If the singularity spectrum $F(\alpha)$ is estimated in a sliding time window, its evolution gives information on the change in the noise structure. In particular, the characteristics of the noise are the position and width

of the support of the spectrum $F(\alpha)$, i.e., the values α_{\min} , α_{\max} , $\Delta\alpha = \alpha_{\max} - \alpha_{\min}$, and α^* , the latter being the value at which $F(\alpha)$ peaks: $F(\alpha^*) = \max_{\alpha} F(\alpha)$. The α^* value is called the generalized Hurst exponent. For a monofractal signal, the $\Delta\alpha$ value must be equal to zero and $\alpha^* = H$. Generally, $F(\alpha^*) = 1$, but it may be that $F(\alpha^*) < 1$ for certain windows. In the general case, $F(\alpha^*)$ is equal to the fractal dimension of support of the multifractal measure [Feder, 1988].

The $\Delta\alpha$ and α^* calculations were based on the following considerations. The exponent q was varied within the interval $q \in [-Q, +Q]$, where Q is a certain quite a large number, say $Q = 10$. For each α within the interval $\alpha \in [A_{\min}, A_{\max}]$ (where $A_{\min} = \min_{q \in [-Q, +Q]} \frac{d\tau(q)}{dq}$, $A_{\max} = \max_{q \in [-Q, +Q]} \frac{d\tau(q)}{dq}$), we calculated the value $\tilde{F}(\alpha) = \min_{q \in [-Q, +Q]} (\alpha q - \tau(q))$. If α is close to A_{\min} , then $\tilde{F}(\alpha) < 0$, and this value cannot be used as an estimate of the singularity spectrum, which must be nonnegative. However, starting from certain α , the $\tilde{F}(\alpha)$ value becomes nonnegative and this condition extracts α_{\min} . As α further increases, the $\tilde{F}(\alpha)$ value grows until reaching maximum at $\alpha = \alpha^*$; then it starts to decrease and, for certain $\alpha > \alpha_{\max}$, where $\alpha_{\max} < A_{\max}$, it again becomes negative: $\tilde{F}(\alpha) < 0$. Thus, we have $F(\alpha) = \tilde{F}(\alpha)$, provided that $\tilde{F}(\alpha) \geq 0$, which determines the interval of the support of the singularity spectrum $\alpha \in [\alpha_{\min}, \alpha_{\max}]$. The derivative $d\tau(q)/dq$ is numerically evaluated according to values $\tau(q)$, $q \in [-Q, +Q]$, and the accuracy of this evaluation does not particularly matter, because it is used just for a crude determination of the a priori interval of the possible exponents q .

A low-frequency microseism analysis below uses estimates of the singularity spectrum in the following successive nonoverlapping time windows: in a window with a length of 30 min (1800 readings) for 1-s data and in a window with a length of 1 day (1440 readings) for 1-min data. The local trends were removed using fourth-order polynomials in the first case and eighth-order polynomials in the second case. The quantity α^* characterizes the most typical and most often encountered Gelder–Lipschitz parameter; $\Delta\alpha$ reflects the diversity of the random signal behavior and, as will be discussed below, this is a kind of measure of the number of hidden degrees of freedom of the stochastic system.

VARIATIONS IN THE WIDTH OF SUPPORT OF THE SINGULARITY SPECTRUM

Figure 2 presents estimates of the singularity spectrum $F(\alpha)$ for one of the windows for 1-s (Fig. 2a) and 1-min (Fig. 2d) data from one (KSK) of the network stations. Moreover, the middle and lower panels show

variations in the parameters α^* and $\Delta\alpha$ during a two-month (July 1 to August 31, 2006) fragment for 1-s (Figs. 2b, 2c) and 1-min (Figs. 2e, 2f) data. Sharp bursts in Figs. 2b and 2c are manifestations of the effects of the onsets of different nearby and remote earthquakes. These bursts are smoothed out in Figs. 2e and 2f after double averaging: first during the passage from a 1-s to 1-min time step and then due to change from 30-min to 1-day windows.

We will consider a set of $\Delta\alpha$ estimates for 1-s data (Fig. 2c). For each 30-min window (within which these estimates were obtained), there are a certain number of stations which provide these estimates on the basis of their data. The number of these stations changes from one two-month fragment to another and, moreover, inside every fragment. For each 30-min window, we calculate a median $\Delta\alpha$ value over all those stations, which contribute data amenable to analysis. The median is a robust (stable to bursts) alternative of the usual average value.

A sequence of the $\Delta\alpha$ medians over all 77 stations (see Fig. 1) compose a single continuous time series with a total length of 14 years with a 30-min time step, which is a kind of integrated statistical characteristic of the microseism field. Exactly same time series can also be obtained separately for each of the five groups of stations in Fig. 1. We will consider how this time series behaves after different smoothing procedures. As a smoothing method, we chose Gaussian trends, which have certain optimal properties [Hardle, 1989]. A Gaussian trend $\bar{X}(t/H)$ of the signal $X(t)$ with the smoothing parameter (radius) $H > 0$ is defined as

$$\bar{X}(t|H) = \frac{\int_{-\infty}^{+\infty} X(t + H\xi)\psi(\xi)d\xi}{\int_{-\infty}^{+\infty} \psi(\xi)d\xi}, \tag{9}$$

$$\psi(\xi) = \exp(-\xi^2).$$

For time series on a discrete timescale, the trend (9) can be efficiently calculated using fast Fourier transform. This averaging method was used to study the geophysical time series in work [Lyubushin, 2007]. Formula (9) suggests that the average value, crudely speaking, refers to the interval centered at t and having the radius H . The $\Delta\alpha$ medians were smoothed using two radii $H = 13$ days and 0.5 yr. The smoothing results for medians over all stations and over 5 clusters are presented in Fig. 3.

One important feature of the behavior of the α values, smoothed for $H = 0.5$ days, is a substantial decline of the average value, which began in early 2003 (a half-year before the event on Hokkaido island); it is noteworthy that the average level reached after this earthquake had no longer recovered until the catastrophe of March 11, 2010. We note that the average $\Delta\alpha$ value

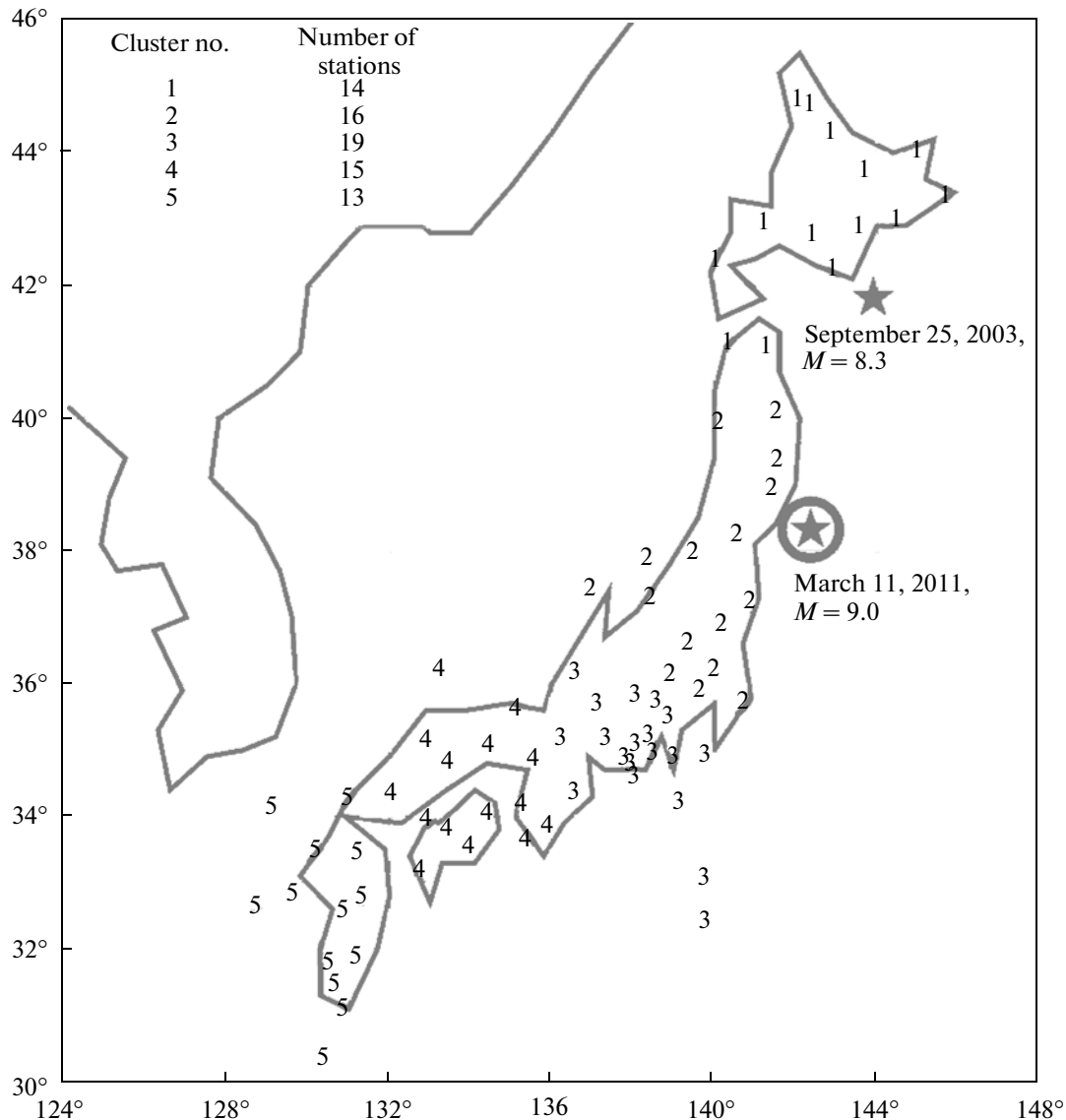


Fig. 1. The positions of 77 broadband seismic stations of the F-net network and their division into five spatial clusters with the number of stations in each cluster indicated. Stars indicate the hypocenters of earthquakes of September 25, 2003 ($M = 8.3$), and March 11, 2011 ($M = 9.0$).

declines no matter which group of the clusters is chosen; this regularity for all network stations was first documented in work [Lyubushin, 2008a], though it was interpreted somewhat later.

The $\Delta\alpha$ value quantifies the diversity of the random signal behavior; therefore, a decrease in $\Delta\alpha$ indirectly indicates that certain degrees of freedom of the medium are suppressed and vanish. At the same time, there may be more direct analogies with a decrease in the number of degrees of freedom manifested in the $\Delta\alpha$ decrease. Works [Pavlov et al., 2003; Ziganshin and Pavlov, 2005] numerically studied the singularity spectra for a sequence of return times in the Poincaré cross

section for systems of two coupled Ressler–Lorentz oscillators.

In the presence of very strong coupling, these oscillators are synchronized, leading to a substantial decrease in the width of the support of the singularity spectrum α . Therefore, the set of results presented in Fig. 3 shows that the field of the microseismic oscillations in Japan after the 2003 event had been synchronized and this state continued until March 11, 2011.

Based on the well-known proposition of catastrophe theory that synchronization is one of the indicators for the coming catastrophe [Gilmore, 1981], works [Lyubushin, 2008b, 2009, 2010d] concluded that the event on Hokkaido island, despite its magni-

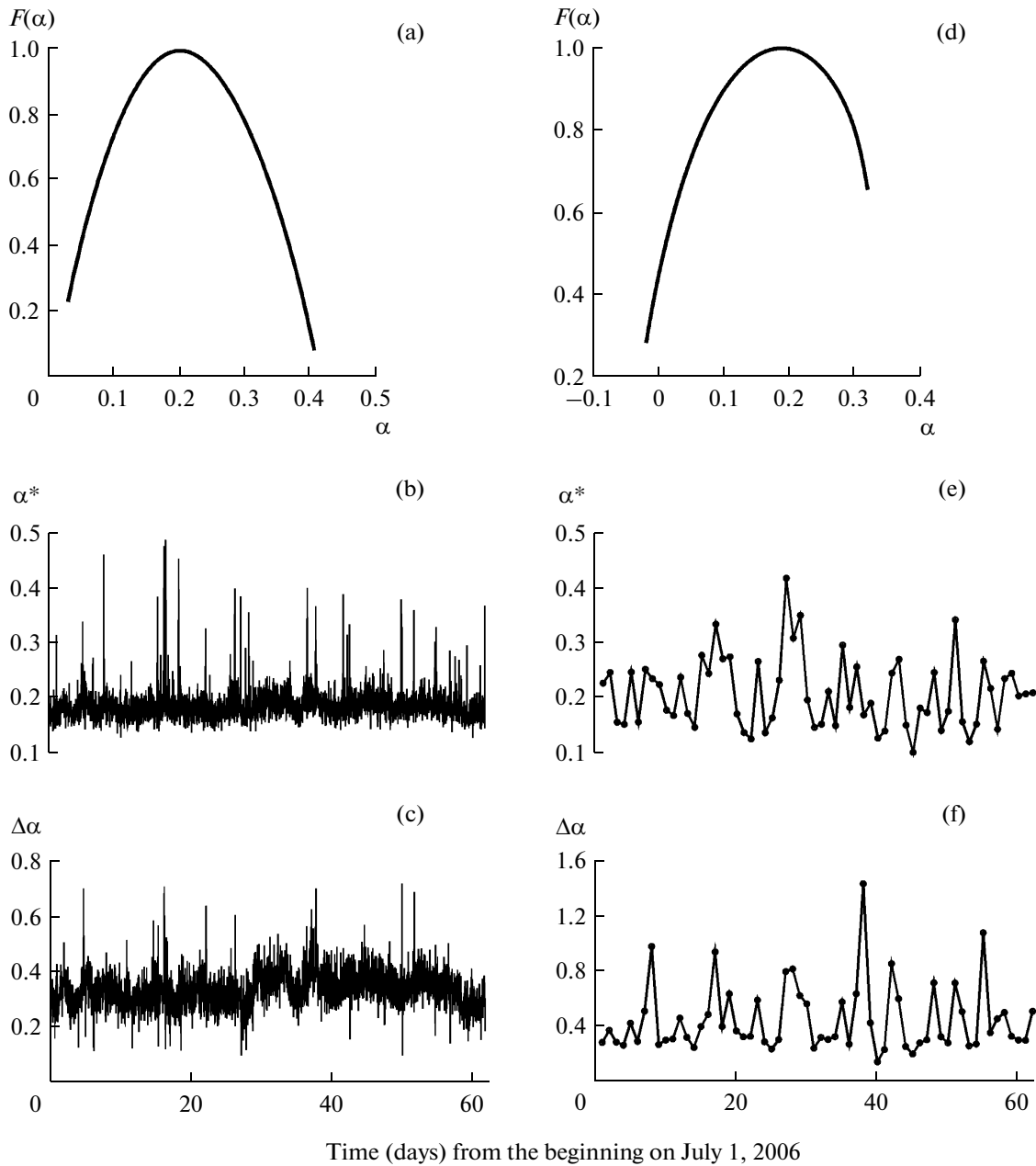


Fig. 2. Estimates of the singularity spectrum $F(\alpha)$ and variations in its parameters (generalized Hurst exponent α^* and the width of the support of the singularity spectrum $\Delta\alpha$) for the KSK station, calculated for the two-month fragment of July 1–August 31, 2006. Calculations are (a, b, c) for 1-s data in successive intervals with a length of 30 min (1800 readings) and (d, e, f) for 1-min data in successive intervals with the length of 1 day (1440 readings). (a, d) Results are for first time intervals with a length of 30 min and 1 day, respectively, for the two-month fragment of July 1–August 31, 2006.

tude ($M = 8.3$), may be merely a foreshock for an even stronger earthquake about to strike the region of Japan. A qualitative estimate of the magnitude of the future shock, $M = 8.5$ – 9.0 , is based just on common sense: the lower bound ($M = 8.5$) relies on the presumption that the magnitude of the primary shock should be larger than the magnitude of the foreshock, and the upper bound ($M = 9.0$) relies on the expectation that that it is not possible to be any stronger.

CORRELATIONS OF OTHER STATISTICS OF THE MICROSEISMIC BACKGROUND

Henceforth, the term “statistic” is taken in the sense of “function of observations” [Cox and Hinkley, 1974]. Below we consider six such statistics, each defined on successive (nonoverlapping) time intervals of a preset length. For microseismic data reduced to a 1-min time step, the length of these intervals is 1 day (1440 readings). Records of microseismic oscillations

contain gaps and instrument failure fragments of differing lengths; therefore, a continuous time series of variations in the studied statistics with a 1-day step was composed by calculating the median of these variations over stations, ensuring acceptable recording as the day goes on.

Thus, we had a set of 30 time series (a product of six parameters multiplied by five clusters of stations) with a uniform 1-day time step. A particular reading in each of these 30 time series results from a sequence of three averaging operations: (1) a direct time averaging, i.e., passing from initial 1-s readings to 1-min readings by taking averages over successive 60 data points; (2) indirect time averaging, performed as an estimation of one or another statistic from 1440 successive 1-min values of microseisms from each station (if available); and (3) spatial averaging of the obtained diurnal estimates of the statistics by taking a median over values from operational stations within a cluster.

Spectral exponent β , smoothness index of the waveform ξ , and logarithm of the variance $\log(\overline{Var})$. The spectral exponent β determines the type of variations in the logarithm of the power spectrum as a function of the logarithm of the period; its value is closely related to the fractal noise characteristics [Feder, 1988; Kantelhardt et al., 2002].

Below, instead of a classical estimation on the basis of Fourier transform or parametrical models, the power spectrum was estimated from the rate of changes in the mean squared absolute values of wavelet coefficients W_k [Mallat, 1998] as functions of detail level number $k = 1, \dots, m$ according to the formula

$$W_k = \sum_{j=1}^{N^{(k)}} |c_j^{(k)}|^2 / N^{(k)}. \quad (10)$$

Here, $c_j^{(k)}$ are the coefficients of an orthogonal discrete wavelet decomposition of a sample of time series ($k = 1, \dots, m$ is the detail level number of decomposition); $N^{(k)}$ is the number of wavelet coefficients at the detail level k , $N^{(k)} \leq 2^{(m-k)}$. Then, by analogy with the formula for the growth rate of the power spectrum, $W_k \sim (s_k)^\beta$, where s_k is a characteristic timescale of the detail level k . Since $s_k = 2^k - 2^{(k+1)}$, we therefore have

$$\log_2(W_k) \sim k^\beta. \quad (11)$$

Thus, the slope of the straight line, fitted to the pairs of the values $(\log_2(W_k), k)$ by the least squares method, gives an estimate of β . The parameter β was estimated in successive time windows with a length of 1440 readings (1 day). This method for calculating the spectral exponents in microseismic noise analysis was used earlier in work [Lyubushin, 2008c]. In order to eliminate the effect of tidal variations, an eighth-order polynomial trend was removed in each window and the wavelet power spectrum (11) and the decimal logarithm of the variance $\log(\overline{Var})$ were calculated for the remainder. For this, we chose an optimal orthogonal

Daubechies wavelet with the number of vanishing moments from 2 to 10, ensuring a minimum of entropy of the distribution of squared wavelet coefficients for the first 7 detail levels of the wavelet decomposition (scales, or “periods,” from 2 to 256 min for the 1-min time step). This method for calculating the spectral exponent automatically gets another useful characteristic, namely, the number ξ of vanishing moments of the optimal wavelet, with possible integer values from 1 to 10. The greater ξ is, the smoother the waveform is within the day.

The abovementioned parameters are calculated for diurnal time intervals at each station where recording for a day is acceptable. Next, the average is taken over all stations of network and over stations within clusters. The medians will be denoted through $\overline{\beta}_r(s)$, $\overline{\log(Var)}_r(s)$, and $\overline{\xi}_r(s)$; here, overbar means spatial averaging (determining the median within a cluster), the subscript $r = 1, \dots, 5$ is the cluster number the median refers to, and the argument s is an integer-valued index which numbers the successive days either from the general beginning of observations (early 1997) or from the beginning of the time window; this is in contrast to the temporal index t , which numbers the successive 1-min readings in seismic records within a day. We note that, after the median is calculated over all the stations, the smoothness index $\overline{\xi}_r(s)$ is no longer an integer number.

The **index of linear predictability** ρ is calculated from the formula $\rho = V_0/V_{AR} - 1$. Here, V_0 is the variance of the error $\varepsilon_0(t+1)$ for the trivial prediction $\hat{x}_0(t+1)$ one step in advance for the increments $x(t)$ of the seismic records, which is equal to the average over the preceding “small” time window with length of n readings: $\hat{x}_0(t+1) = \sum_{s=t-n+1}^t x(s)/n$. Thus, $\varepsilon_0(t+1) = x(t+1) - \hat{x}_0(t+1)$ and $V_0 = \sum_{t=n+1}^N \varepsilon_0^2(t)/(N-n)$, where $N > n$ is the number of readings in successive “large” time fragments. The V_{AR} value is calculated from a similar formula $V_{AR} = \sum_{t=n+1}^N \varepsilon_{AR}^2(t)/(N-n)$. Here, $\varepsilon_{AR}(t+1) = x(t+1) - \hat{x}_{AR}(t+1)$ is the error of the linear prediction $\hat{x}_{AR}(t+1)$ one step in advance with the help of the second-order autoregression model (AR prediction), whose coefficients are calculated from the preceding “small” time window with the length of n readings. That is, we consider the model

$$x(t) + a_1 x(t-1) + a_2 x(t-2) = e(t) + d, \quad (12)$$

where $c = (a_1, a_2, d)^T$ is a vector of unknown parameters which are determined from the sliding “small” window with the length of n readings from the condition of the minimum of the sum of squares of discrepancies $e(t)$. We introduce the vector $Y(t) =$

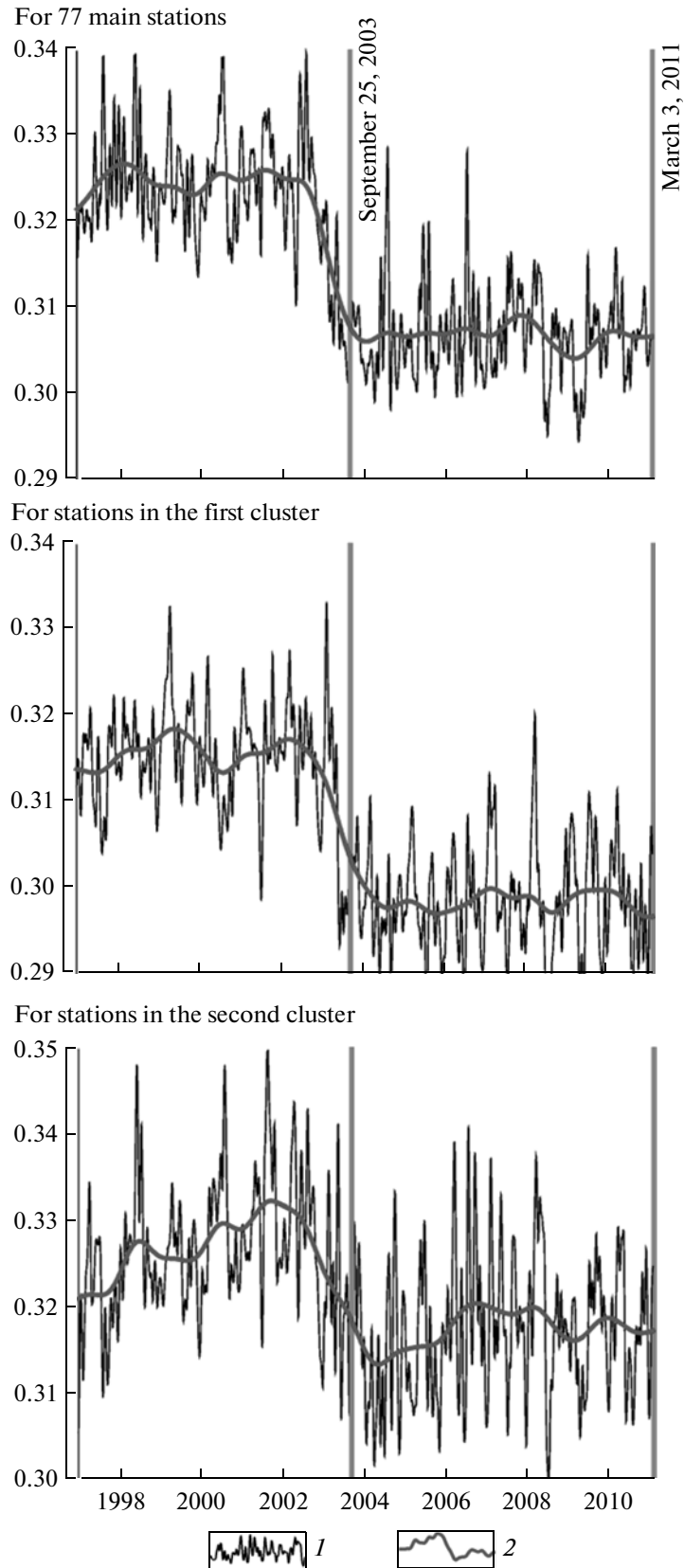


Fig. 3. Smoothed medians of the estimated width of the support of the multifractal singularity spectrum $\Delta\alpha$ in successive time windows with a length of 30 min for the initial vertical seismic records with a discretization frequency of 1 Hz. Gaussian kernel smoothing in a window with a radius of 13 days (curve 1) and 0.5 years (curve 2). Here and in Figs. 3–6, 8, and 10, the vertical lines correspond to the times of the earthquakes of September 25, 2003 ($M = 8.3$) and March 11, 2011 ($M = 9.0$).

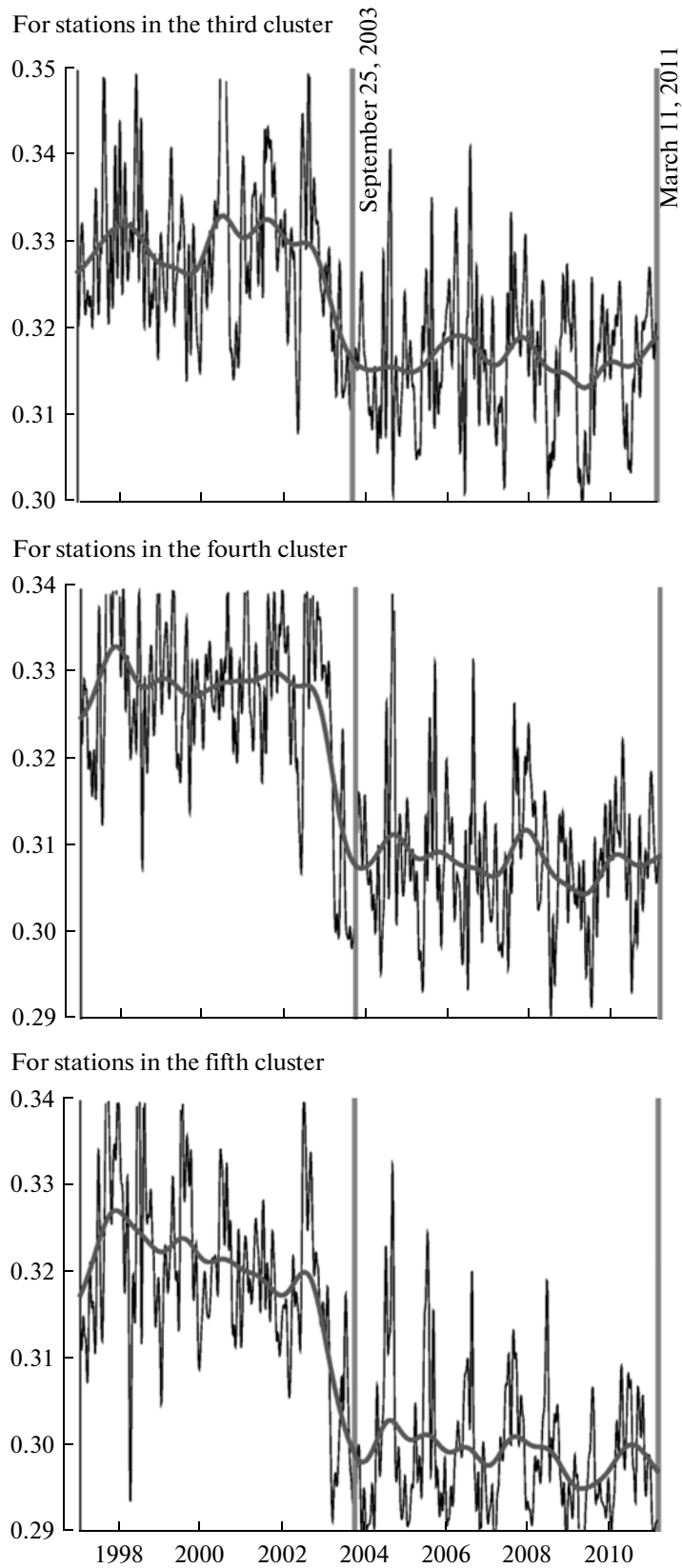


Fig. 3. (Contd.).

$(-x(t-1), -x(t-2), 1)^T$. Then, the autoregression model can be succinctly written as $x(t) = c^T Y(t) + e(t)$.

In order to calculate the prediction one step in advance $\hat{x}_{AR}(t+1)$, we will determine the vector c from the condition of the minimum of the sum of squares of the discrepancies $e(t)$ according to n preceding readings:

$$\sum_{\lambda=t-n+3}^t e^2(\lambda) = \sum_{\lambda=t-n+3}^t (x(\lambda) - c^T Y(\lambda))^2 \rightarrow \min_c,$$
 from this we can easily obtain the formulas for estimating the vector of parameters and prediction one step in advance by the least squares method:

$$\begin{aligned} \hat{c}(t) &= A^{-1}(t)R(t), \quad A(t) = \sum_{\lambda=t-n+3}^t Y(\lambda)Y^T(\lambda), \\ R(t) &= \sum_{\lambda=t-n+3}^t x(\lambda)Y(\lambda), \end{aligned} \quad (13)$$

$$\hat{x}_{AR}(t+1) = x(t+1) - \hat{x}^T(t)Y(t).$$

The second order of the autoregression was chosen because it is the minimum order for an AR model that enables a description of the oscillation motion and admits the positioning of the maximum of the spectral density within a frequency range between the Nyquist frequency and zero frequency [Box and Jenkins, 1970; Kashyap and Rao, 1976]. We changed to increments to escape the dominance of low frequencies (tidal component and other trends). The AR prediction uses a correlation property between neighboring increments in records which, if it exists, yields $V_{AR} < V_0$ and $\rho > 0$.

Below, the index of the linear predictability ρ for 1-min data was always estimated in successive "long" time windows with a length of $N = 1440$ readings (1 day) and in "short" window with a length of $n = 60$ readings (1 h).

Other than the two abovementioned parameters of the multifractal singularity spectrum, $\Delta\alpha$ and α^* , we will also analyze the quantity $\gamma = \alpha^* - (\alpha_{\min} + \alpha_{\max})/2$, which characterizes the skewness of the singularity spectrum.

By analogy with the abovementioned notations $\bar{\beta}_r(s)$, $\overline{\log(Var)}_r(s)$ and $\bar{\xi}_r(s)$, we will denote through $\bar{\rho}_r(s)$, $\bar{\alpha}_r^*(s)$, $\overline{\Delta\alpha}_r(s)$ and $\bar{\gamma}_r(s)$ the medians of the corresponding statistics, where the overbar means the operation of taking the median, the argument s numbers the successive days, and index $r = 1, \dots, 5$ numbers the clusters of the stations.

Robust multiple correlation measure κ . We will briefly consider the procedure of calculating a measure which describes the multiple (total) correlation between components of multidimensional time series. It is based on the use of canonic correlations [Hotelling, 1936; Rao, 1965], but differs from the classical approach by employing robust (stable to bursts) estimates. This procedure was described in detail in work

[Lyubushin, 2007]. Suppose that $u_r(s)$, $r = 1, \dots, Q$ is the Q -dimensional time series and $s = 1, \dots, L$ is the discrete time.

In our case, $Q = 5$ (the number of clusters of the stations); $u_r(s)$ are median diurnal values $\bar{\beta}_r(s)$, $\overline{\log(Var)}_r(s)$, $\bar{\rho}_r(s)$, $\bar{\alpha}_r^*(s)$, $\overline{\Delta\alpha}_r(s)$, and $\bar{\gamma}_r(s)$; s is the index which numbers the successive days; and L is the total number of successive days which are analyzed simultaneously (to be set subsequently to either 91 (one-fourth of the year) or 365 (1 year)).

We select a component with the number p and consider the linear regression model of the effect of all the other components on the chosen component u_p :

$$u_p(s) = w_p(s) + \varepsilon_p(s), \quad w_p(s) = \sum_{r=1, r \neq p}^Q \gamma_r^{(p)} u_r(s). \quad (14)$$

The regression coefficients $\gamma_r^{(p)}$ are found from the condition of the minimum of the sum of absolute values $\sum_{s=1}^L |\varepsilon_p(s)|$, and then the correlation coefficient μ_p between the selected component $u_p(s)$ and the resulting regression contribution $w_p(s)$ is estimated according to the formula of the robust estimate of the correlation coefficient [Huber, 1981]:

$$\mu_p = (S(\widehat{\bar{z}}_p^2) - S(\widetilde{\bar{z}}_p^2)) / (S(\widehat{\bar{z}}_p^2) + S(\widetilde{\bar{z}}_p^2)), \quad (15)$$

where $\widehat{\bar{z}}_p(t) = a_p u_p(s) + b_p w_p(s)$, $\widetilde{\bar{z}}_p(s) = a_p u_p(s) - b_p w_p(s)$, $a_p = 1/S(u_p)$, $b_p = 1/S(w_p)$, and $S(u_p) = \text{med}|u_p - \text{med}(u_p)|$. Here, $\text{med}(u_p)$ means the median of the sample $u_p(s)$, $s = 1, \dots, L$, and $S(u_p)$ is thus the absolute median deviation of the sample $u_p(s)$. The use of robust estimates, i.e., the minimization of the sum of the moduli of the regression residuals $\varepsilon_p(s)$ rather than their squares (which are much easier to compute), as well as the use of formula (15) to estimate the correlation coefficient, are motivated by the need for the μ_p estimates to be stable in reaction to large bursts caused by nearby small and moderate and distant strong earthquakes.

The μ_p value will be called the robust canonical correlation [Hotelling, 1936; Rao, 1965] between the p th component and all the other components. We make calculations successively for all $p = 1, \dots, Q$ and then determine the quantity

$$\kappa = \prod_{p=1}^Q |\mu_p|, \quad (16)$$

which will be called a robust multiple measure of the correlation of multidimensional time series.

It is evident that $0 \leq \kappa \leq 1$; the closer the value defined in (16) is to unity, the stronger the general relation is between the variations in the components of the time series $u_p(s)$. By evaluating formula (16) for the sliding time window of the preset length of L readings

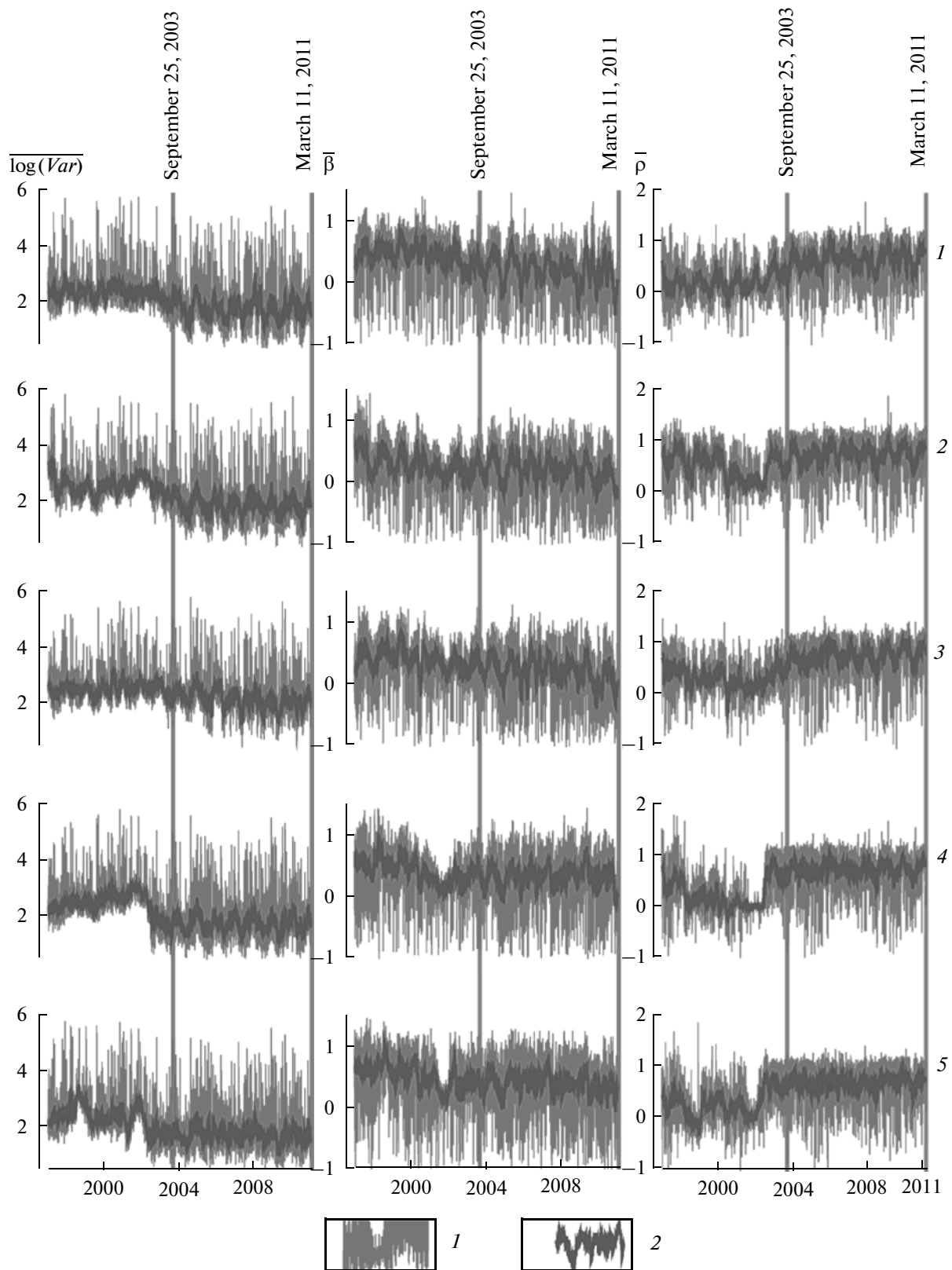


Fig. 4. Variations in the medians of statistics of microseismic noise from different groups of stations. Behaviors of the medians $\overline{\log(Var)}$ of the decimal algorithms of the variance, spectral exponents $\bar{\beta}$, and the linear predictability indices $\bar{\rho}$ (calculated for the stations within the five clusters whose positions are illustrated in Fig. 1; the cluster numbers are given on the right of the panels) for 1-min seismic records (curve 1) and their averages in the sliding time window with a radius of 14 days (curve 2). Calculations are in successive time windows with a length of 1440 readings (1 day).

with the time mark of the right-hand end of the sliding window τ instead of for the entire sample, we will obtain the evolution of the multiple correlation (16) in the form of dependence $\kappa(\tau/L)$. According to the number of the used statistics of the diurnal time fragments, there will be six of these dependences; in writing, the second argument L will be dropped for simplicity: $\kappa_{\beta}(\tau)$, $\kappa_{\log(Var)}(\tau)$, $\kappa_{\rho}(\tau)$, $\kappa_{\alpha^*}(\tau)$, $\kappa_{\Delta\alpha}(\tau)$, and $\kappa_{\gamma}(\tau)$. We also note that the quantities defined in (15) and (16) were calculated not for the initial data, but rather for the increments of the median values in order to ensure more stationarity of the samples analyzed.

The median values of the six statistics used are plotted in Figs. 4 and 5. They behave quite randomly and irregularly. Therefore, Figs. 4 and 5 present time averages (curve 2) of the initial median values over the sliding window with a radius of 14 days. These averages often show strongly pronounced seasonal (annual) variations.

It should be noted that, despite the fact that the characteristics presented in Figs. 4 and 5 have quite synchronous annual variations, the general low-frequency decreasing trend of the median values $\overline{\log(Var)}$ is accompanied by a similar general increasing trend of the linear predictability index $\bar{\rho}$. This tendency is most apparent for the fourth and fifth clusters in the time interval of late 2002 to early 2003. It is noteworthy that $\bar{\rho}_4$ and $\bar{\rho}_5$ values show considerable and quite sharp spikes in July 2002, which seems to be due to beginning of the growth of synchronization. As plotted, the growth of the linear predictability index means increases in the time correlation between microseismic oscillations. The median $\bar{\rho}$ grows rather slowly for three northern clusters and shows jump-like variations for two southern clusters. The medians of the spectral exponents $\bar{\beta}$ often have maxima in summer months and minima in winter months, i.e., the microseisms have a lower frequency character in summer than in winter.

Figure 6 presents the variations in the robust multiple measure of correlation κ for all statistics. Measure (16) was calculated for two time windows (91 days and 365 days). We note that the use of the one-year window for calculating the measure of the correlation is equivalent to averaging the seasonal effects of cyclones, storms, and hurricanes as the main generators of low-frequency microseisms; as a consequence, the estimate is very smooth and stable (cf. Fig. 6, curves 1, 2). The main feature of these dependences is that the magnitude of the multiple correlation coefficient grows before the event of September 25, 2003, and levels off to a new higher level until March 11, 2011.

The analysis performed in [Lyubushin, 2010d] showed that the extraction of the synchronization

effects becomes very stable and statistically significant due to the use of long (1-year) time windows. Thus, independent analysis (through the use of not only the parameters of the singularity spectra) confirmed the main conclusion of the work [Lyubushin, 2009] that the parameters of the field of low-frequency microseisms for the islands of Japan had been synchronized after the earthquake of September 25, 2009, on Hokkaido island; moreover, the time of the beginning of the systematic growth of synchronization, namely, July 2002, could be quite exactly indicated due to the use of a new statistic, namely, the linear predictability index.

CLUSTER ANALYSIS OF THE PARAMETERS OF LOW-FREQUENCY MICROSEISMIC BACKGROUND

Estimates of multiple measures of correlation in sliding time windows, which were used in works [Lyubushin, 2009, 2010d] and presented above, failed to identify any other significant anomalies in the behavior of the parameters of the microseism field during observations in 1997–2010, let alone a relatively rapid passage to the high synchronization level in the second half of 2002 through the beginning of 2003. Below we use another method of data analysis, namely, the cluster analysis of the cloud of background-parameter vectors in a sliding window with a length of 2 years. The initial purpose of this analysis is to answer the question of how many “behavioral modes” of microseismic background can be identified and how rapidly the number of these modes changes with time. Here, the behavioral mode is taken to mean a cluster (a compact group) of parameter vectors in a current “long” two-year window. This approach, used in work [Lyubushin, 2011], allowed us to introduce a new parameter, namely, the “cluster exponent” μ , and to identify an anomalous fragment of the behavior of the background in 2007–2010; this episode was characterized by a positive trend of the μ values, which was analogous to a shorter trend before the event of September 25, 2003, on Hokkaido island. This approach does not divide the network stations into a prescribed number of spatial groups for a subsequent calculation of the measures of coherence or correlation between variations in different background parameters within each group of stations in sliding time windows as described in works [Lyubushin, 2009, 2010d]. Thus, the medians of the parameters of background are taken over all network stations; therefore, the parameters used are integrated characteristics of the microseism field in the region covered by the observation network.

Figure 7 presents the variations in the medians for all seven considered statistics: $\bar{\beta}$, $\bar{\xi}$, $\overline{\log(Var)}$, $\bar{\rho}$, $\bar{\alpha}^*$, $\bar{\Delta\alpha}$, and $\bar{\gamma}$ together with their average values in the sliding window with a length of 57 days, which was

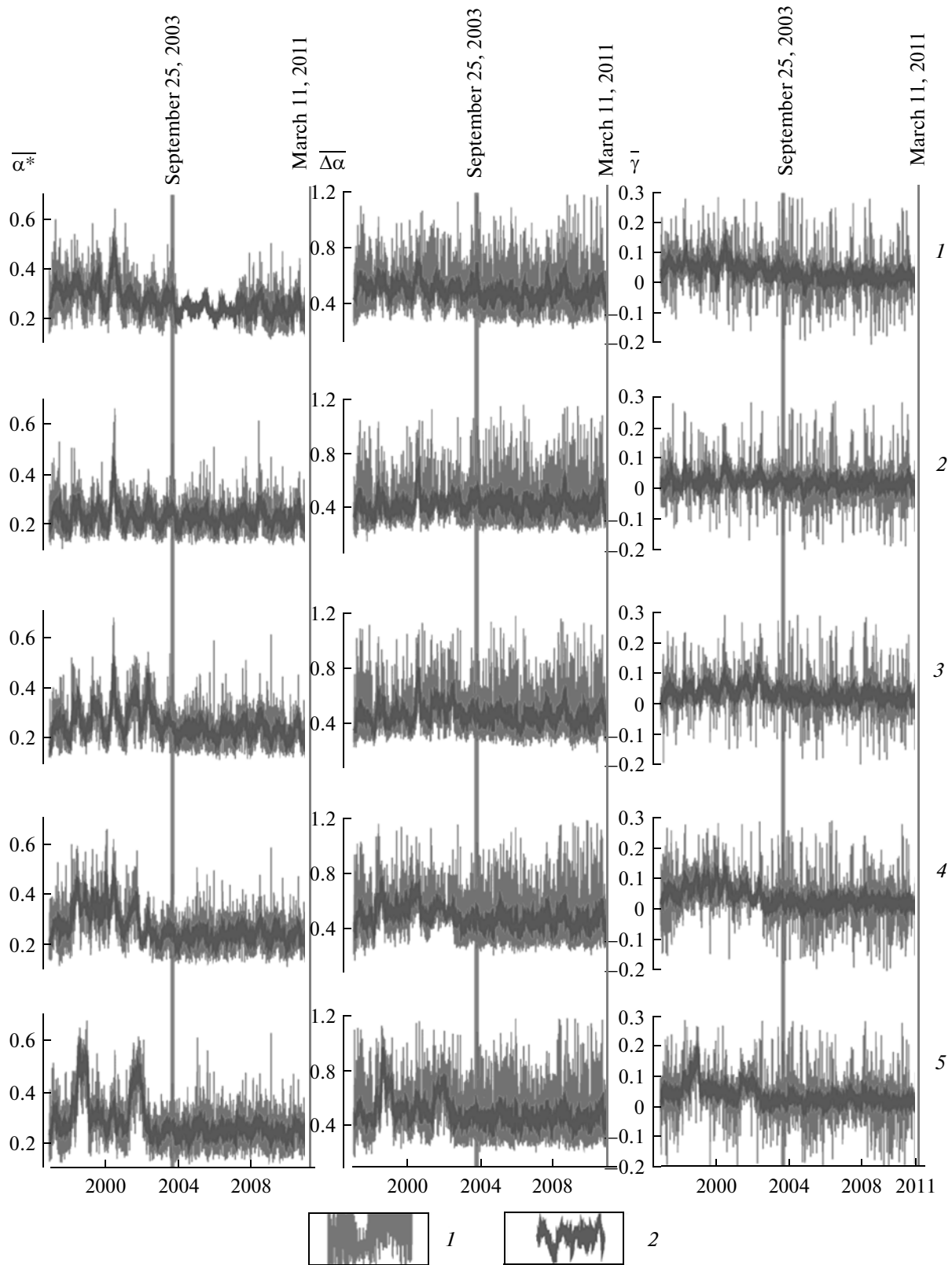


Fig. 5. Variations in the medians of $\bar{\alpha}^*$, $\overline{\Delta\alpha}$, $\bar{\gamma}$ of microseismic noise from different groups of stations. Behaviors of the medians $\bar{\alpha}^*$, $\overline{\Delta\alpha}$, $\bar{\gamma}$ of multifractal singularity spectra calculated for the stations within five clusters whose positions are illustrated in Fig. 1 (cluster numbers are given on the right of each panel) for 1-min seismic records (curve 1) and their averages in a sliding time window with a radius of 14 days (curve 2). The singularity spectra were calculated within successive time windows with a length of 1440 readings (1 day).

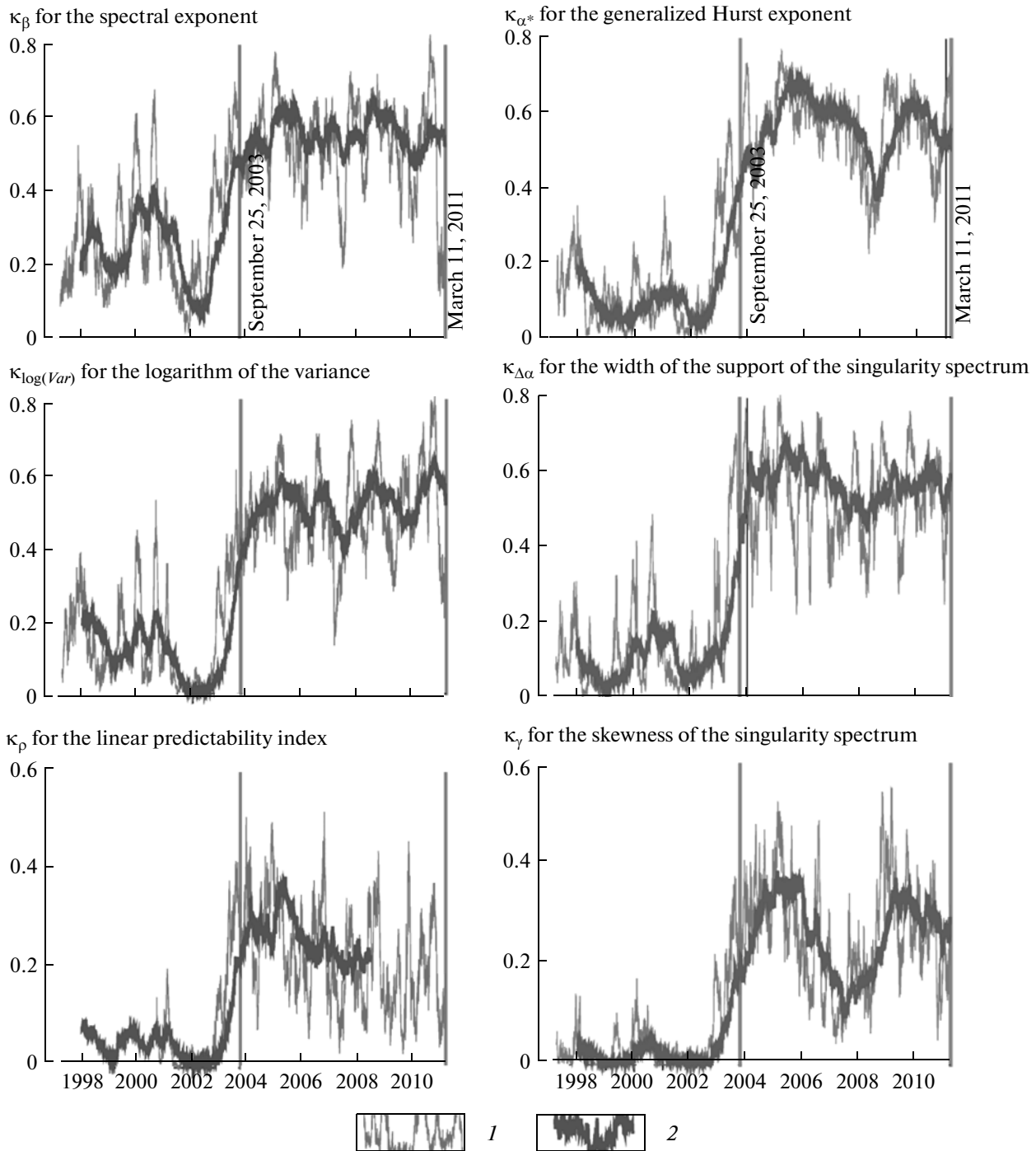


Fig. 6. Robust multiple measure of correlation κ estimated for the increments of medians of statistics $\bar{\beta}$, $\overline{\log(Var)}$, $\bar{\rho}$, $\bar{\alpha}^*$, $\bar{\Delta\alpha}$, and $\bar{\gamma}$ (subscripts for κ) calculated for seismic stations within five spatial clusters (see Fig. 1) for 1-min data over successive days. The estimates of κ in a window with a length of 0.25 yr (91 reading, curve 1) and 1 yr (365 readings, curve 2).

chosen to be equal to two lunar months (28 days is the period of modulation of many geophysical processes) plus one day, in order to get an odd value of the length of the sliding averaging window.

Figure 8 presents variations in the correlation coefficient (16) between two parameters $\bar{\alpha}^*(s)$ and $\bar{\Delta\alpha}(s)$

calculated in a sliding time window with a length of 1 year. Figure 8 is notable in that it displays two prominent anomalies in the behavior of the correlation coefficient: sharp minima in 2002 and 2009. The first anomaly of 2002 was followed by the large earthquake of September 25, 2003; therefore, it was logical to expect that the second sharp minimum of the correla-

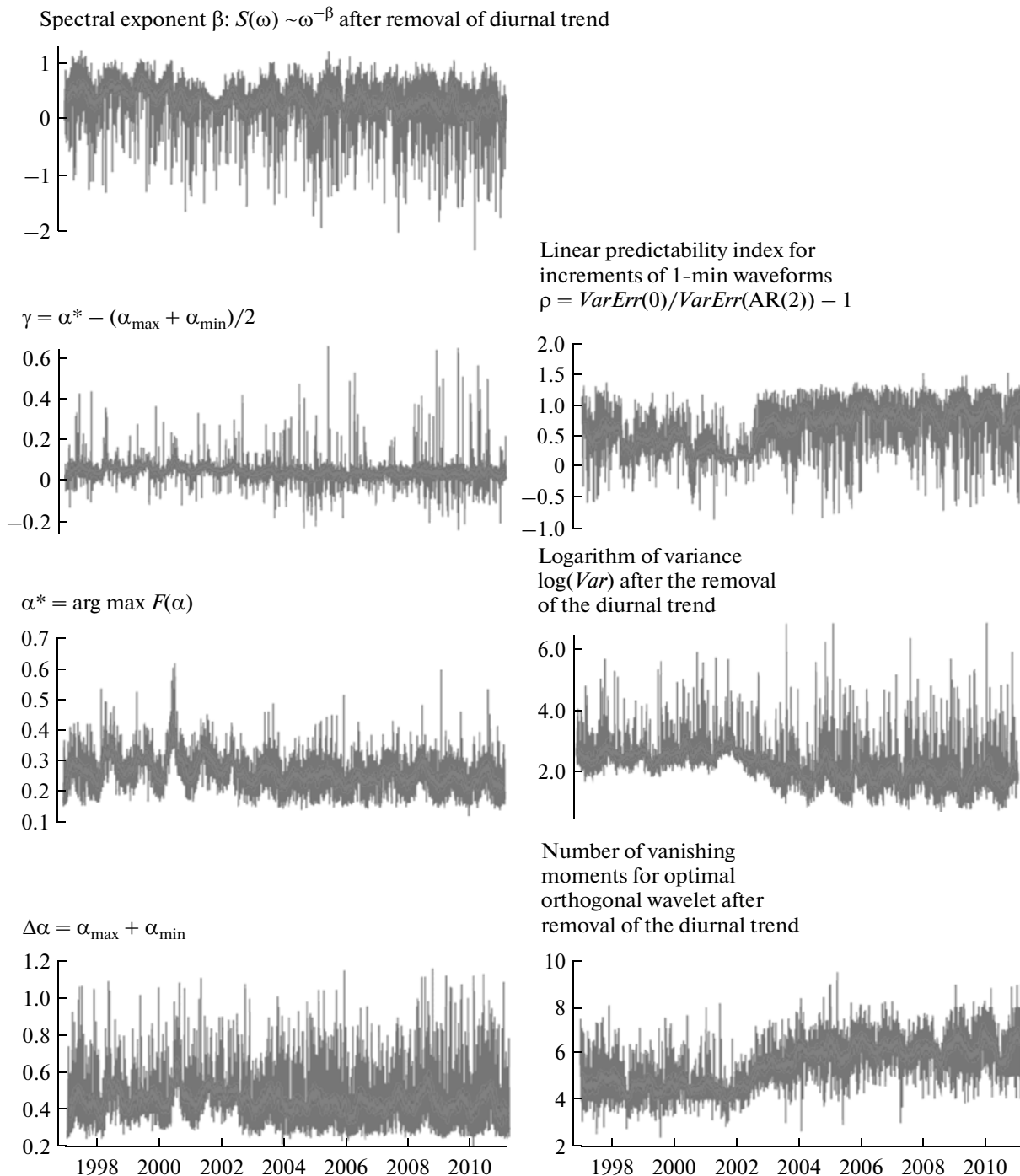


Fig. 7. Dependences of the statistics, which were calculated as medians over all seismic stations of the F-net network in successive time windows with a length of 1 day: the spectral exponent β , skewness of the singularity spectrum γ , generalized Hurst exponent α^* , the width of the support of the singularity spectrum $\Delta\alpha$, linear predictability index ρ , decimal logarithm of the variance $\log(\text{Var})$, and waveform smoothness index ξ . The β , $\log(\text{Var})$, and ξ were calculated after detrending with the help of an 8-order polynomial in each window with the length of 1 day. Thick lines show 57-day running averages.

tion coefficient could also be a precursor to a future strong (and, possibly, even higher energy) event in the second half of 2010. From this dependence we could conclude [Lyubushin, 2010b, c, 2011] that, starting from mid-2010, a strong event with $M = 8.5-9.0$ should be expected on the islands of Japan.

Next, a sliding time window with a length of 730 days (2 years) was taken and the following sequence of operations for a cloud of 7-dimensional vectors $\vec{\psi}$ with components $\bar{\beta}$, $\bar{\xi}$, $\overline{\log(\text{Var})}$, $\bar{\rho}$, $\bar{\alpha}^*$, $\bar{\Delta\alpha}$, and $\bar{\gamma}$ was performed within every window:

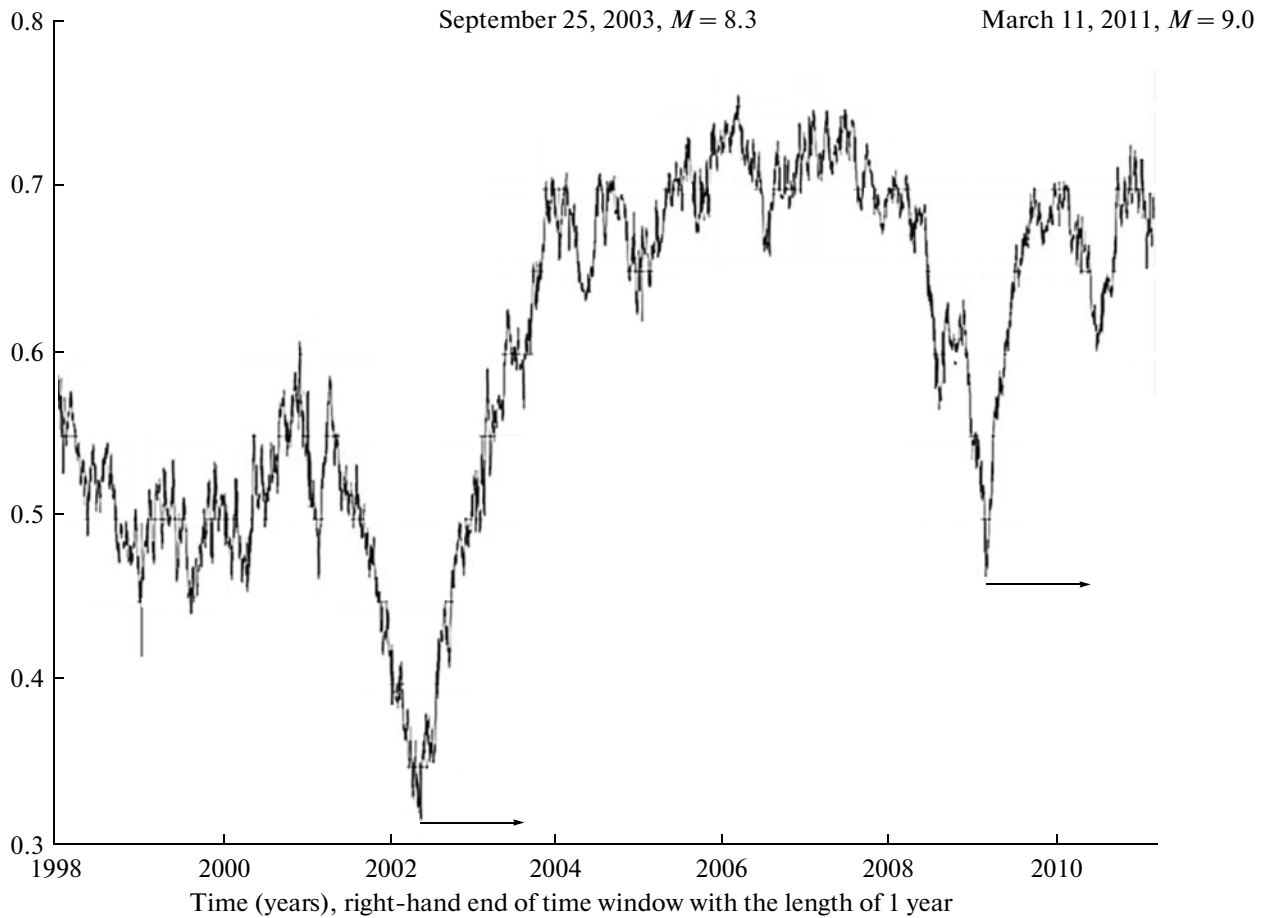


Fig. 8. Robust correlation coefficient between variations in $\bar{\alpha}^*$ and $\overline{\Delta\alpha}$ (see Fig. 6) in 365-day (1-year) sliding time window as a function of the position of the right-hand end of the time window. Arrows indicate same-length time intervals from the time of the first “downspike” of the correlation coefficient to the time of earthquake of March 25, 2009, and from the time of the second downspike to July 2010, estimated as the beginning of the dangerous catastrophe expectation time interval.

(1) each component of the vector $\vec{\psi}$ was subject to the operation of normalization and winsorization: we calculated the sampling average values and standard deviations σ , subtracted the sampling values, cut out the values outside of $\pm 4\sigma$, and divided the result by σ ; this was iterated until σ no longer changed;

(2) for the cloud of normalized 7-dimensional vectors thus obtained, we calculated the first four principal components as projections of the covariance matrix onto the eigenvectors within a current window, the eigenvectors being chosen to correspond to four maximum eigenvalues (which ensured extra noise suppression and retained from 91 to 95% of the total variance);

(3) for the obtained cloud of 4-dimensional vectors of the principal components, a division into a given number q of clusters Γ_k , $k = 1, \dots, q$, was performed. The trial number of clusters varied successively from 40 to 2. The division was performed using a sequence of hierarchical clustering with the use of the “farthest neighbor” metric (which yielded compact and “round”

clusters), followed by iterations of the K -means method [Duda and Hart, 1973].

Let N be the total number of 4-dimensional vectors $\vec{\zeta}$ of principal components (of normalized 7-dimensional vectors) in the current time window and $\vec{\zeta}_0$ be the vector of the general center of mass of a cloud of principal components (here, $\vec{\zeta} = 0$, due to the preliminary operations of normalization and winsorization); $\vec{\zeta}_k$, $k = 1, \dots, q$ are the vectors of the centers of mass of the clusters and n_k is the number of elements in each cluster, $\sum_{k=1}^q n_k = N$. The division of a cloud of N vectors into a preset number q of clusters is estimated according to the following formulas:

$$\sigma_0^2(q) = \frac{\sum_{k=1}^q \sum_{\zeta \in \Gamma_k} |\vec{\zeta} - \vec{\zeta}_k|^2}{N - q} \quad (17)$$

is the measure of intracluster compactness;

$$\sigma_1^2(q) = \frac{\sum_{k=1}^q v_k |\xi_k - \xi_0|^2}{q-1}, \quad v_k = \frac{n_k}{N} \quad (18)$$

is the weighted measure of the discrepancy between the centers of the clusters; and

$$PFS(q) = \frac{\sigma_1^2(q)}{\sigma_0^2(q)} \quad (19)$$

is the so-called pseudo-*F*-statistic [Vogel and Wong, 1978].

A cloud is divided into q clusters to minimize the value of $\sigma_0^2(q)$. The $\sigma_0^2(q)$ value can also be formally determined for $q = 1$: $\sigma_0^2(1) = \sum_{\xi} |\xi - \xi_0|^2 / (N - 1)$.

The $\sigma_0^2(q)$ value increases with a decrease of q , and $\log(\sigma_0^2(q))$ depends nearly linearly on $\log(q)$, i.e., $\sigma_0^2(q) \sim q^{-\mu}$.

This fact is illustrated in Fig. 9. The μ value will be called the cluster exponent. For a given window, this exponent can be estimated as the slope of a least square fit of the dependence $\log(\sigma_0^2(q))$ on $\log(q)$.

Formula (19) characterizes the quality of division into a given number of clusters: the greater $PFS(q)$ is, the better the division is.

For a good division, the intracluster compactness $\sigma_0^2(q)$ should be small and the discrepancy $\sigma_1^2(q)$ between clusters should be large. An optimal number of clusters q^* is found from the condition of maximum of $PFS(q)$. At the same time, $PFS(q)$ (and, more specifically, $\sigma_1^2(q)$) cannot be calculated for $q = 1$. Therefore, some other considerations are required in order to distinguish between $q = 1$ and $q = 2$. It is well known that the optimal number of clusters can also be determined from the breakpoint of the monotonic dependence $\sigma_0^2(q)$ for $q = q^*$: the function $\sigma_0^2(q)$ grows faster with a decrease in q for $q < q^*$ than for $q > q^*$. This criterion of $q = q^*$ determination is more sensitive to noise interference and performs worse than the method $q^* = \arg \max_{2 \leq q} PFS(q)$; however, it is the only possible method to distinguish between the cases when $q = 1$ and when $q = 2$. Through $\delta \log(\sigma_0^2(q))$, we denote the deviation of the $\log(\sigma_0^2(q))$ value from the best fit of the dependence on $\log(q)$. Then point $q = 2$ will be considered the breakpoint of the $\sigma_0^2(q)$ dependence if $\delta \log(\sigma_0^2(1))$ exceeds all $\delta \log(\sigma_0^2(q))$ values for $q \geq 2$. Based on the aforesaid, the optimal number q^* of clusters will be defined as follows:

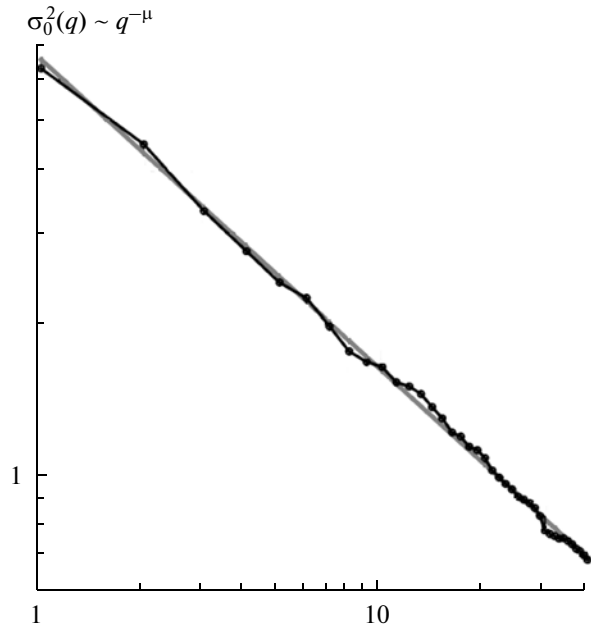


Fig. 9. Dependence that the functional of intracluster compactness $\sigma_0^2(q)$ has on the trial number of clusters q . The straight line is the best linear fit of the dependence that $\log(\sigma_0^2(q))$ has on $\log(q)$.

Suppose that $q_0 = \arg \max_{2 \leq q \leq 40} PFS(q)$,

if $q_0 > 2$, then $q^* = q_0$;

otherwise, if $\delta \log(\sigma_0^2(1)) \leq \max_{2 \leq q \leq 40} \delta \log(\sigma_0^2(q))$, (20)

then $q^* = 1$;

otherwise $q^* = 2$.

Figure 10 presents the results of clustering the four principal components of 7 diurnal median characteristics of the microseismic background from F-net network for 14 years of observations (1997–2010), estimated in a sliding time window with a length of two years ($N = 730$) with a time shift of 7 days.

From Fig. 10 we can conclude that the character of switching between the numbers of optimal clusters became more chaotic after 2004, and the option of three optimal clusters, which was dominant before 2004, totally disappeared after 2004. This fact can be interpreted as a “freezing” of a certain internal degree of freedom in the microseism field after the event of September 25, 2003, before the upcoming strong shock of March 11, 2011.

The cluster exponent μ follows a well-defined linear trend, reaches a maximum, and returns to a new average level before the event of September 25, 2003; the latter is in sharp contrast to the initial background of statistical fluctuations around the average value. This cluster exponent again starts following the linear trend when the right-hand side of the two-year win-

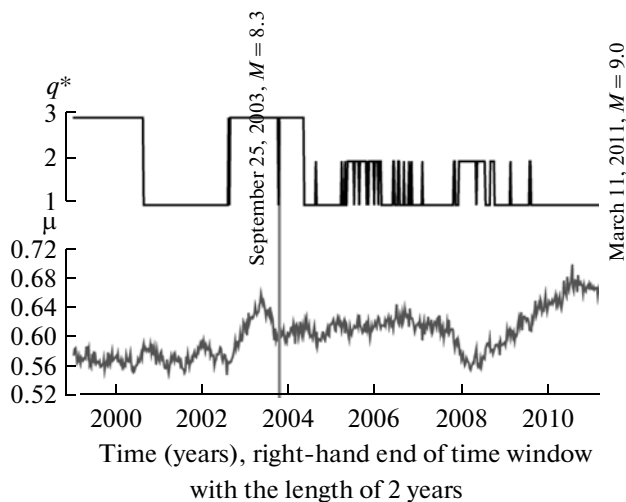


Fig. 10. Results of a cluster analysis of the four first principal components in a sliding time window with the length of two years with a shift of 7 days as a function of the position of the right-hand end of time window: q^* is the optimal number of clusters and μ is the cluster exponent.

dow is at early 2008, but now this positive trend is much longer. Like the shorter term linear trend before the event of September 25, 2003, now the more extended increasing linear trend of the cluster exponent again ends with a local maximum followed by a decline starting a half-year before the powerful earthquake of March 11, 2011.

CONCLUSIONS

An analysis of low-frequency microseismic noise identified long-term precursors of the seismic catastrophe of March 11, 2011, in Japan. It should be noted that the traditional earthquake prediction methods, based on an analysis of the specific features of the flux of small to moderate magnitude seismic events before previous strong earthquakes did not detect two successive catastrophes with magnitude of $M = 9$ in Sumatra on December 26, 2004, and in Japan on March 11, 2011. This may be due to the absence of sufficient statistics to learn the algorithms for predicting the strongest earthquakes in view of their small number. This necessitates the creation and maintenance of quite densely arranged routine geophysical monitoring networks like F-net in Japan whose data should be freely accessed via Internet.

ACKNOWLEDGMENTS

This work was supported by the Russian Fund for Basic Research (through grant no. 09-05-00134).

REFERENCES

- Berger, J., Davis, P., and Ekstrom, G., Ambient Earth Noise: A Survey of the Global Seismographic Network, *J. Geophys. Res.*, 2004, vol. 109, p. B11307.
- Box, G.E.R. and Jenkins, G.M., *Time Series Analysis. Forecasting and Control*, San Francisco, Cambridge, London, Amsterdam: Holden-Day, 1970; Moscow: Mir, 1974.
- Cox, D.R. and Hinkley, D.V., *Theoretical Statistics*, London: Chapman and Hall, 1974; Moscow: Mir, 1978.
- Currenti, G., del Negro, C., Lapenna, V., and Telesca, L., Multifractality in Local Geomagnetic Field at Etna Volcano, Sicily (Southern Italy), *Natural Hazards Earth Syst. Sci.*, 2005, vol. 5, pp. 555–559.
- Duda, R.O. and Hart, P.E., *Pattern Classification and Scene Analysis*, New York: Wiley, 1973; Moscow: Mir, 1976.
- Ekstrom, G., Time Domain Analysis of Earth's Long-Period Background Seismic Radiation, *J. Geophys. Res.*, 2001, vol. 106, no. B11, pp. 26483–26493.
- Feder, J., *Fractals*, New York: Plenum Press, 1988; Moscow: Mir, 1989.
- Friedrich, A., Krüger, F., and Klinge, K., Ocean-Generated Microseismic Noise Located at the Gräfenberg Array, *J. Seismol.*, 1998, vol. 2, no. 1, pp. 47–64.
- Gilmore, R., *Catastrophe Theory for Scientists and Engineers*, New York: Wiley, 1981; Moscow: Mir, 1984.
- Hardle, W., *Applied Nonparametric Regression*, Cambridge: Univ. Press, 1989; Moscow: Mir, 1993.
- Hotelling, H., Relations between Two Sets of Variates, *Biometrika*, 1936, vol. 28, pp. 321–377.
- Huber, P.J., *Robust Statistics*, New York: Wiley, 1981; Moscow: Mir, 1984.
- Ida, Y., Hayakawa, M., Adalev, A., and Gotoh, K., Multifractal Analysis for the ULF Geomagnetic Data during the 1993 Guam Earthquake, *Nonlin. Proc. Geophys.*, 2005, vol. 12, pp. 157–162.
- Kantelhardt, J.W., Zschiegner, S.A., Konsciency-Bunde, E., Havlin, S., Bunde, A., and Stanley, H.E., Multifractal Detrended Fluctuation Analysis of Non-stationary Time Series, *Phys. A*, 2002, vol. 316, pp. 87–114.
- Kashyap, R.L. and Rao, A.R., *Dynamic Stochastic Models from Empirical Data*, New York: Acad. Press, 1976; Moscow, Nauka, 1983.
- Kobayashi, N. and Nishida, K., Continuous Excitation of Planetary Free Oscillations by Atmospheric Disturbances, *Nature*, 1998, vol. 395, pp. 357–360.
- Kurrle, D. and Widmer-Schmidrig, R., Spatiotemporal Features of the Earth's Background Oscillations Observed in Central Europe, *Geophys. Rev. Lett.*, 2006, vol. 33, p. L24304.
- Lyubushin, A.A. and Sobolev, G.A., Multifractal Measures of Synchronization of Microseismic Oscillations in a Minute Range of Periods, *Izv. Phys. Solid Earth*, 2006, vol. 42, no. 9, pp. 734–744.
- Lyubushin, A.A., *Analiz dannykh sistem geofizicheskogo i ekologicheskogo monitoringa* (Data Analysis of Geophysical and Ecological Monitoring Systems), Moscow: Nauka, 2007.
- Lyubushin, A.A., Mean Multifractal Properties of Low-Frequency Microseismic Noise, in *Proc. 31st General*

- Assembly of the European Seismological Commission ESC—2008*, Hersonissos, Crete, Sept. 7–12, 2008a, pp. 255–270.
- Lyubushin, A.A., Microseismic Noise in Minute Period Range: Properties and Possible Prognostic Features, *Izv. Phys. Solid Earth*, 2008c, vol. 44, no. 4, pp. 275–290.
- Lyubushin, A.A., Multifractal Properties of Low-Frequency Microseismic Noise in Japan, 1997–2008, in *Proc. 7th General Assembly of the Asian Seismological Commission and Japan Seismological Society. Fall Meeting*, Tsukuba, Nov. 24–27, 2008b, p. 92.
- Lyubushin, A.A., Synchronization Trends and Rhythms of Multifractal Parameters of the Field of Low-Frequency Microseisms, *Izv. Phys. Solid Earth*, 2009, vol. 45, no. 5, pp. 381–394.
- Lyubushin, A., Multifractal Parameters of Low-Frequency Microseisms, in *Synchronization and Triggering: from Fracture to Earthquake Processes, GeoPlanet: Earth and Planetary Sciences*, Berlin: Springer, 2010b, chapter 15, pp. 253–272. doi: 10.1007/978-3-642-12300-9_15
- Lyubushin, A.A., Synchronization of Multifractal Parameters of Regional and Global Low-Frequency Microseisms, *European Geosciences Union General Assembly 2010*, Vienna, May 2–7, 2010a; *Geophys. Res. Abstr.*, 2010a, vol. 12, abstr. EGU2010-696.
- Lyubushin, A.A., Synchronization Phenomena of Low-Frequency Microseisms, *Proc. 32nd European Seismological Commission General Assembly*, Montpellier, Sept. 6–10, 2010b, p. 124.
- Lyubushin, A.A., The Statistics of the Time Segments of Low-Frequency Microseisms: Trends and Synchronization, *Izv. Phys. Solid Earth*, 2010d, vol. 46, no. 6, pp. 544–554.
- Lyubushin, A.A., Cluster Analysis of the Properties of Low-Frequency Microseismic Noise, *Izv. Phys. Solid Earth*, 2011, vol. 47, no. 6.
- Mallat, S.A., *A Wavelet Tour of Signal Processing*, San Diego Academic Press, 1998; Moscow: Mir, 2005.
- Mandelbrot, B.B., *The Fractal Geometry of Nature*, New York: Freeman, 1982; Moscow: Inst. Komp'yut. Issled., 2002.
- Pavlov, A.N., Sosnovtseva, O.V., and Mosekilde, E., Scaling Features of Multimode Motions in Coupled Chaotic Oscillators, *Chaos, Solitons, Fractals*, 2003, vol. 16, pp. 801–810.
- Ramírez-Rojas, A., Muñoz-Diosdado, A., Pavía-Miller, C.G., and Angulo-Brown, F., Spectral and Multifractal Study of Electrostatic Time Series Associated to the $M_w = 6.5$ Earthquake of 24 Oct. 1993 in Mexico, *Natural Hazards Earth Syst. Sci.*, 2004, vol. 4, pp. 703–709.
- Rao, C.R., *Linear Statistical Inference and Its Applications*, New York: John Wiley and Sons, 1965; Moscow: Nauka, 1968.
- Rhie, J. and Romanowicz, B., Excitation of Earth's Continuous Free Oscillations by Atmosphere–Ocean–Seafloor Coupling, *Nature*, 2004, vol. 431, pp. 552–554.
- Rhie, J. and Romanowicz, B., A Study of the Relation between Ocean Storms and the Earth's Hum—G3: Geochemistry, Geophysics, Geosystems, *Electron. J. Earth Sci.*, 2006, vol. 7, no. 10, Available from: <http://www.agu.org/journals/gc/>
- Stehly, L., Campillo, M., and Shapiro, N.M., A Study of the Seismic Noise from Its Long-Range Correlation Properties, *J. Geophys. Res.* 2006, vol. 111, p. B10306.
- Tanimoto, T., Um, J., Nishida, K., and Kobayashi, N., Earth's Continuous Oscillations Observed on Seismically Quiet Days, *Geophys. Res. Lett.*, 1998, vol. 25, pp. 1553–1556.
- Tanimoto, T. and Um, J., Cause of Continuous Oscillations of the Earth, *J. Geophys. Res.*, 1999, vol. 104, no. 28, pp. 723–739.
- Tanimoto, T., Continuous Free Oscillations: Atmosphere–Solid Earth Coupling, *Ann. Rev. Earth Planet. Sci.*, 2001, vol. 29, pp. 563–584.
- Tanimoto, T., The Oceanic Excitation Hypothesis for the Continuous Oscillations of the Earth, *Geophys. J. Int.*, 2005, vol. 160, pp. 276–288.
- Taqqu, M.S., Self-Similar Processes, in *Encyclopedia of Statistical Sciences*, New York: John Wiley and Sons, 1988, vol. 8, pp. 352–357.
- Telesca, L., Colangelo, G., and Lapenna, V., Multifractal Variability in Geoelectrical Signals and Correlations with Seismicity: a Study Case in Southern Italy, *Natural Hazards Earth Syst. Sci.*, 2005, vol. 5, pp. 673–677.
- Vogel, M.A. and Wong, A.K.C., PFS Clustering Method, *IEEE Trans. Pattern Anal. Mach. Intell.*, 1978, vol. PAMI1-5, pp. 237–245.
- Ziganshin, A.R. and Pavlov, A.N., Scaling Properties of Multimode Dynamics in Coupled Chaotic Oscillators, *Proc. 2nd Int. Conf. "Physics and Control"*, St. Petersburg, Aug. 24–26, 2005, pp. 180–183.